A Climate Data Record of Stratospheric Aerosols

Viktoria F. Sofieva[1], Alexei Rozanov[2], Monika Szelag[1], John P. Burrows[2], Christian Retscher[3], Robert Damadeo[4], Doug Degenstein[5], Landon A. Rieger[5] and Adam Bourassa[5]

[1]Finnish Meteorological Institute, Helsinki, Finland
[2]University of Bremen, Bremen, Germany
[3] ESA-ESRIN, Frascati, Italy
[4] NASA Langley Research Center, Hampton, VA, USA
[5] Institute of Space and Atmospheric Studies, University of Saskatchewan, Saskatoon, Canada

Correspondence to: Viktoria F. Sofieva (viktoria.sofieva@fmi.fi)

Abstract. Climate-related studies need information about the distribution of stratospheric aerosols, which influence the energy balance of the Earth's atmosphere. In this work, we present a merged dataset of vertically resolved stratospheric aerosol extinction coefficients, which is derived from data by six limb and occultation satellite instruments: SAGE II on ERBS, GOMOS and SCIAMACHY on Envisat, OSIRIS on Odin, OMPS on Suomi-NPP, and SAGE III on the International Space Station.

The merging of aerosol profiles is performed by transformation of the aerosol datasets from individual satellite instruments to the same wavelength 750 nm and their de-biasing and homogenization by adjusting the seasonal cycles. After such homogenization, the data from individual satellite instruments are in good agreement. The merged aerosol extinction coefficient is computed as the median of the adjusted data from the individual instruments.

The merged time series of vertically resolved monthly mean aerosol extinction coefficients at 750 nm is provided in 10° latitudinal bins from 90°S to 90°N, in the altitude range from 8.5 km to 39.5 km. The time series of the stratospheric aerosol optical depth (SAOD) is created by integration of aerosol extinction profiles from the tropopause to 39.5 km; it is also provided as monthly mean data in 10° latitudinal bins. The created aerosol climate record covers the period from October 1984 until December 2023, and it is intended to be extended in the future. It can be used in various climate-related studies.

1   Introduction

Stratospheric aerosols play an important role in the Earth system and in the climate. Through the scattering of solar radiation back to space and by heating the stratosphere through the absorption of thermal infrared radiation upwelling from the troposphere, stratospheric aerosols impact the radiative forcing and thus the energy balance of the Earth's atmosphere. By providing a surface for heterogeneous reactions, which release halogens, stratospheric aerosols contribute to the catalytic depletion of ozone. Because of a strong coupling between stratospheric aerosols, stratospheric ozone amount, and thermal

balance and dynamics of the atmosphere, it is essential to consider realistic aerosol information in modelling studies and interpretation of the measurements related to the stratosphere. The information about stratospheric aerosols and their influence on climate is also of value for investigations and analyses relevant for geoengineering (e.g., Crutzen, 2006).

One of the characteristics widely used to describe the amount of stratospheric aerosol is its extinction coefficient[1]. As discussed e.g. by von Savigny et al. (2015), at a first approximation the aerosol extinction coefficient can be used to estimate the radiative forcing and thus quantify the impact of aerosols on climate change. There are several data sets of the stratospheric aerosol extinction coefficient retrieved from satellite measurements in limb-viewing geometry (e.g., Bourassa et al., 2012; Damadeo et al., 2013; von Savigny et al., 2015; Vanhellemont et al., 2010; Loughman et al., 2018). The first joint analysis of aerosol records from multiple instruments has been done by Vernier et al. (2011), but this study did not aim at creating a long-term merged data set. A merged time series of the aerosol extinction coefficient using SAGE (Stratospheric Aerosol and Gas Experiment) II and OSIRIS (Optical Spectrograph and InfraRed Imaging System) aerosol data was presented by Rieger et al. (2015). The merging approach was based on a simple scaling of the extinctions at different wavelengths assuming a prescribed wavelength dependence characterized by a fixed value of the Ångström exponent. The latter represents a drawback of the method as the Ångström exponent might vary significantly even in the absence of very strong volcanic eruptions (e.g., Malinina et al., 2019). The GloSSAC aerosol climatology presented by Thomason et al. (2018) is an extension of the climatology described by Rieger et al. (2015) including the earlier observations from 1979 to 1984, extending the coverage of the data set during the SAGE II measurement period and adding CALIPSO (Cloud-Aerosol Lidar and Infrared Pathfinder Satellite Observation) observations after 2006. This climatology uses, however, the same conversion of the OSIRIS data to SAGE II wavelengths as described by Rieger et al. (2015). The updated version of GloSSAC (Kovilakam et al., 2020) includes the latest versions of the individual aerosol dataset and added SAGE III aerosol extinction on International Space Station (ISS), which allows an improved conversion of aerosol extinction to other wavelengths to be made.

This paper describes a merged long-term dataset of aerosol extinction coefficient profiles at 750 nm derived from data by solar/stellar occultation and limb-scatter instruments: SAGE II on ERBS (Earth Radiation Budget Satellite), GOMOS (Global Ozone Monitoring by Occultation of Stars) and SCIAMACHY (Scanning Imaging Spectrometer for Atmospheric Chartography) on Envisat, OSIRIS on Odin, OMPS-LP (Ozone Monitor Profiling Suite Limb Profiler) on Suomi-NPP, and SAGE III on ISS (International Space Station). This dataset is referred to as Climate Data Record of Stratospheric Aerosols (CREST) hereafter. Our objective is to increase the reliability of the data set by including the extinction measurements from multiple instruments measuring similar atmospheric quantities in the limb-viewing geometry in the post-SAGE II period

The paper is organized as follows. Section 2 is dedicated to short descriptions of aerosol datasets from individual satellite instruments. Section 3 presents the merging algorithm. The correction and filling gaps on SAGE II data during the high

---

[1] The extinction coefficient is the sum of absorption and scattering in the atmosphere along the radiation path per unit distance. It is equal to $\sum N_i(\sigma_{a,i}(\lambda) + \sigma_{s,i}(\lambda))$, where N_i is the number density of atmospheric constituent i, $\sigma_{a,i}(\lambda)$ is the absorption coefficient of species i at wavelength λ, $\sigma_{s,i}(\lambda)$ is the scattering coefficient of species i at wavelength λ.

volcanic load after the Pinatubo eruption is discussed in Section 4. Creating stratospheric optical depth is discussed in Section 5. Illustrations of the merged dataset and its comparison with GloSSAC v2.21 are presented in Section 6. Summary and discussion (Section 7) conclude the paper.

2   Satellite aerosol data

65   For creating the CREST merged dataset, we used aerosol profiles from several limb and occultation instruments. The information about individual datasets is summarised in Table 1. Below we present also the   descriptions of individual aerosol datasets.

Table 1. Information about the datasets used in the CREST dataset.

Instrument/ satellite	Processor, references	Time period	Local time	Vertical resolution	Profiles per day	Wavelength(s) for aerosol retrievals
SAGE II/ ERBS	NASA v7.0 (Damadeo et al., 2013)	Oct 1984 – Aug 2005	sunrise, sunset	~1 km	14–30	386, 452, 525 and 1020 nm
OSIRIS/ Odin	USask v7.2 (Rieger et al., 2019)	Nov 2011 – present	6 a.m., 6 p.m.	~2 km	~250	750 nm
GOMOS/ Envisat	FMI-GOMOSaero v.1 (Sofieva et al., 2024)	Aug 2002 – Dec 2011	10 p.m.	3 km	monthly mean values	400, 440, 452, 470, 500, 525, 550, 672 and 750 nm
SCIAMACHY/ Envisat	UBr v3.0 (von Savigny et al., 2015; Rieger et al., 2018; Malinina et al., 2019	Aug 2002- Apr 2012	10 a.m.	~3 km	~1300	750 nm
OMPS-LP/ Suomi NPP	UBr v2.1 (Rozanov et al., 2024)	Apr 2012–present	1:30 p.m.	~2 km	~1600	869 nm
SAGE III /ISS	NASA, AO3 v5.3 (Wang et al., 2020)	2017 – present	sunrise, sunset	~1 km	~30	384, 449, 520, 602, 676, 756, 869, 1021, and 1544 nm

70   **2.1   OSIRIS**

OSIRIS on board the Odin satellite(Llewellyn et al., 2004, p.200) performs limb-scatter measurements of the atmosphere from 2001 to present. In our work we use the cloud-cleared aerosol extinction profiles from new v7.2 retrievals (Rieger et al., 2019). The v7.2 processor uses wavelengths at 470, 675, 750 and 805 nm to retrieve aerosol extinction at 750 nm. The retrievals have reduced measurement geometry biases and improve extinction retrieval in the upper troposphere and lower stratosphere,

75 compared to the previous v5.10 retrieval algorithm. The OSIRIS v7.2 aerosol extinction profiles are provided at 750 nm in the vertical range from ~6.5 km up to 35 km with the vertical resolution of ~ 2 km. According to the recommendations of the OSIRIS team, post-2022 data are not used in the merged dataset.

2.2 SAGE II

SAGE II was a solar occultation instrument that operated on board the ERBS satellite from 1984-2005
80 (https://sage.nasa.gov/missions/about-sage-ii/, Russell and McCormick, 1989). SAGE II had seven channels at ultraviolet, visible, and infrared wavelengths. The aerosol retrieval algorithm provides information about the size distribution, composition, and concentration of the aerosols (Thomason et al., 2008). In our analyses, we used v7 aerosol data. The detailed description of aerosol retrievals can be found in (Damadeo et al., 2013). SAGE II aerosol extinction profiles are provided at 386, 452, 525 and 1020 nm in the stratosphere and in the upper troposphere with the vertical resolution of ~ 1.0 km.

85 We applied the following cloud filtering of individual SAGE II profiles. The cloud altitude is defined at location where aerosol extinction at 1020 nm $\beta_{1020\,nm} \geq 2.5 \cdot 10^{-3}\,km^{-1}$ and ratio of extinctions $\frac{\beta_{525\,nm}}{\beta_{1020\,nm}} \leq 1.75$. Each profile was examined for presence of clouds; if found, all data at and below 1 km above that altitude are excluded. These criteria are slight modifications of various previous simplistic cloud-filtering techniques applied to SAGE data (e.g., Damadeo et al., 2024; Davis et al., 2021; Wang et al., 2002).

2.3 SAGE III/ISS

90 SAGE III is a solar occultation instrument currently operating on board the ISS; it was installed in 2017 (https://www-sage3-iss.larc.nasa.gov/). The SAGE III detectors cover from the ultraviolet to the near-infrared parts of the spectrum, and they allow for the characterization of different types of aerosols in the atmosphere. The retrieval methodology is similar to that of SAGE II, albeit with more spectral channels to better constrain the shape of the aerosol extinction spectrum (Wang et al., 2020). In
95 our analyses, we used v5.3 aerosol data.
SAGE III/ISS aerosol extinction profiles are provided at 9 wavelengths (384, 449, 520, 602, 676, 756, 869, 1021, and 1544 nm) in the altitude range from cloud top to ~45 km with the vertical resolution of ~ 0.75 km. The SAGE III/ISS data are filtered for presence of clouds in the same way as SAGE II data.

2.4 SCIAMACHY

100 The SCIAMACHY instrument was part of the payload of the ESA Envisat (Bovensmann et al., 1999; Burrows et al., 1995) launched on the 28th of February 2002 into a sun-synchronous orbit, with an equator crossing time of 10:00 am in a descending node. It made measurements, including those during its commissioning phase from March 2002 to April 2012 when Envisat failed. During each orbit, measurements in the following three observation modes were made: nadir, limb, and solar/lunar occultation. Of relevance to this study are the measurements made in the limb viewing geometry, which achieve global

105   coverage in 6 days at the equator. These are used to retrieve aerosol extinction profiles (Malinina et al., 2019; Rieger et al., 2018; von Savigny et al., 2015). We note that, in addition, solar occultation measurements were also made (see Noel et al., 2020) close to the terminator in the northern hemisphere but have limited latitude coverage.

In the limb measurement mode, the SCIAMACHY entrance optics, which include two scan mirrors and a telescope, collect the solar radiance upwelling from the atmosphere. The latter comprises the radiance scattered towards SCIAMACHY, i.e., a)

110   that passes through the atmosphere en route to the surface and b) that is scattered back by the surface or clouds and then scattered by the atmosphere. In the standard limb scan mode, as opposed to an alternative optimized for measurements in the mesosphere and lower stratosphere, the SCIAMACHY optical scanner unit register vertical profiles of the scattered radiance from a tangent point, close to or just below the surface, to a tangent height of ~100 km.

The vertical scanning was done with a sampling of about 3.3 km. The instantaneous field of view of the instrument was about

115   2.6 km. At each tangent height, a horizontal scan with typically 4 measurements and a total swath of 960 km was performed. The spectral coverage of SCIAMACHY was 214 - 2386 nm with spectral resolution varying from 0.2 to 1.5 nm. In this study, Level 1 data (Version 8) provided by ESA are used, along with the utilization of calibration flags 1, 2, 4, 5, and 7. These flags address, respectively, the amount of leakage current, the pixel-to-pixel gain, stray-light correction, wavelength calibration, and radiometric calibration.

120   The aerosol extinction coefficients used in this study are from the University of Bremen processor V3.0, which is a further development of the V1.4 processor described by Rieger et al. (2018). Similar to the V1.4 aerosol extinction product, the retrieval is performed at 750 nm. The retrieval is done iteratively using the Levenberg-Marquardt approach. The regularization is applied to the relative differences with respect to the prior profile with a priori standard deviation set to 50. The main differences between V3.0 and V1.4 include the use of sun-normalized radiance instead of normalization to a limb measurement

125   at an upper tangent height and the utilization of an effective surface albedo retrieved from collocated nadir measurements. The latter approach is similar to that used by Pohl et al. (2024), however, the effective surface albedo is based solely on the collocated nadir observations and is not changed any more when retrieving the aerosol extinction profile. In addition, the vertical range of the retrieval is extended to 9 – 38 km in comparison with 12 - 35 km in V1.4. The validation results for V3.0 extinction retrieval show that the agreement with SAGE II data is similar to that found with V1.4 data products. However,

130   most of the outliers identified in the comparison of V1.4 extinction data with independent measurements are not seen in the comparisons for the V3.0 product anymore.

2.5   GOMOS

GOMOS is a stellar occultation instrument operated on board Envisat satellite in 2002-2012 (Bertaux et al., 2010; Kyrölä et al., 2004). GOMOS measured stellar light in the occultation geometry from above the atmosphere until the star lost in the field

135   of view, typically at altitudes 10-15 km. In our analyses, we use the aerosol data retrieved with the FMI-GOMOSaero v1.0 processor (Sofieva et al., 2024), which uses monthly and zonally averaged nighttime transmittance spectra as a basis for aerosol retrievals. The inversion algorithm uses the same strategy as GOMOS retrievals of trace gases: the spectral inversion

followed by the vertical inversion (Kyrölä et al., 2010). The spectral inversion relies on removal of contribution from ozone, NO_2, NO_3 and Rayleigh scattering from the optical depth spectra, for each ray perigee altitude. The FMI-GOMOSaero dataset

140   v.1.0 provides aerosol extinction profiles in the altitude range 10-40 km at wavelengths 400, 440, 452, 470, 500, 525, 550, 672 and 750 nm with a vertical resolution of 3 km.

2.6   OMPS-LP

OMPS-LP is a part of the OMPS instrument suite operating on board the Suomi-NPP satellite of NOAA/NASA since the end of 2011 (Flynn et al., 2014). The field of view of the OMPS-LP instrument is pointed tangentially to the Earth's surface (limb-

145   viewing geometry) and collects spectral radiance scattered by the Earth's atmosphere and reflected by the underlying surface by using a two-dimensional charged-coupled device (CCD). The atmosphere is observed in the tangent height range from 0 to 100 km with a vertical sampling of 1 km and vertical field of view of each pixel of about 1.5 km. The spectral coverage of the OMPS-LP instrument is 280 - 1000 nm with a spectral resolution increasing from 1 nm in the UV region to about 30 nm in the near-IR. In this study, Level 1 data V2.6 provided by NASA are used. Only measurements from the central slit are

150   considered.

The aerosol extinction coefficients used in this study are from the University of Bremen product V2.1, which is described in details in Rozanov et al. (2024). Briefly, the aerosol extinction coefficients are retrieved at a wavelength of 869 nm using the sun-normalized radiance in the tangent height range from 8.5 to 48.5 km. The retrieval is iterative and uses the Levenberg-Marquardt approach with Tikhonov regularization (zeroth order term and first order derivative). At each iteration, the vertical

155   profile of the aerosol extinction coefficient and the effective surface albedo are estimated simultaneously using all measurements in the selected tangent height range. The regularization is done with respect to the solution at the previous iteration.

3   Merged dataset of aerosol profiles

The datasets from individual satellite instruments – GOMOS, OMPS-LP, OSIRIS, SAGE II, SAGE III/ISS, SCIAMACHY –

160   were collected and gridded as monthly zonal means with 10° step in the latitude. OSIRIS dataset was selected as the reference because it has the longest data record. As OSIRIS dataset is available only at 750 nm, this wavelength was chosen as the reference wavelength. The merging procedure consists of (i) conversion of data to 750 nm, if they are retrieved at another wavelength, (ii) data adjustment and (iii) merging adjusted aerosol profiles from different instruments. Below we describe the details of each processing step.

3.1 Conversion to 750 nm

The extinction data, retrieved from the observations of the other instruments, were converted to the wavelength of 750 nm, if not already retrieved at this wavelength. For the conversion of SAGE II data, we used aerosol extinction at 525 nm and 1020 nm. The conversion is based on the Ångström formula

$$\beta_\lambda = \beta_{\lambda_0} \left(\frac{\lambda}{\lambda_0}\right)^{-\alpha}, \tag{1}$$

where β_λ and β_{λ_0} are aerosol extinction coefficients at wavelengths λ and λ_0, and α is the Ångström exponent, with a correction derived from SAGE III/ISS data (for details, see Damadeo et al., 2023):

$$\beta_{750\,nm} = \beta_{1020\,nm} \left(\frac{750}{1020}\right)^{-\alpha} (1.23 - 0.055\alpha). \tag{2}$$

In Eq.(2), the Ångström exponent α is determined using the SAGE II aerosol extinction data at 525 and 1020 nm. . This correction accounts for the bias introduced when using the Angstrom exponent for interpolation as the aerosol extinction spectrum does not quite follow the Angstrom formula.

GOMOS 675-nm aerosol data were converted to 750 nm using the Ångström exponent, which was determined from GOMOS 500 and 675 nm aerosol extinction coefficients. As no measurement data providing the Ångström exponent for the entire operation period of OMPS-LP are available, the Ångström exponent used to convert OMPS-LP data was obtained by Mie calculations assuming a fixed particle size distribution, PSD (r_{med} = 0.08 μm, σ = 1.6). When scaling from 869 to 750 nm wavelength this corresponds to a constant factor of 1.477. The fixed PSD assumed here is the same as used in the OMPS-LP retrieval procedure and based on an arbitrarily selected balloon-borne in-situ measurement presented by Deshler (2008).

3.2 Data adjustment

Gridded time series from individual instruments were compared and methods to remove biases between the time series were analyzed. The datasets have biases with respect to each other, and seasonal cycles also differ at some locations and altitude levels (top panels of Figures 1, 2 and Figures S1-S4 of the Supplement).

SCIAMACHY, OMPS-LP and GOMOS are adjusted to the OSIRIS time series as follows. For each instrument i, latitude zone and altitude level, the seasonal cycle $S_i(m)$, m is a month, is estimated using volcanic-free periods (years 2001-2005, 2007, 2010, 2013-2016, 2020). Then the seasonal cycles are fitted to the OSIRIS seasonal cycle using a robust linear regression

$$S_{OSIRIS}(m) = a + b \cdot S_i(m) + \epsilon \tag{3}$$

In Eq.(3), a and b are the fitted coefficients and ϵ is noise. This procedure ensures that the scaling is performed properly even in cases where not full year is covered by OISRIS data. The original seasonal cycles of SCIAMACHY, OMPS-LP and GOMOS are replaced with fitted seasonal cycles:

$$\beta_{corr,i} = \beta_i - S_i + (a + b \cdot S_i), \tag{4}$$

where S_i is the values for the seasonal cycle at the corresponding month.

For SAGE II and SAGE III/ISS, due to limited data sampling and a relatively short overlapping period with OSIRIS, the seasonal cycle correction is not performed. For these datasets, the offset is computed as the median difference between OSIRIS and occultation aerosol data in their overlapping periods (the period is 2017-2021 for SAGE III and 2001-2005 for SAGE II) and added to data. The adjustment procedure works well, also in complicated cases.

200 ## 3.3   The merging procedure and uncertainty estimates

The merged aerosol extinction coefficient time series is calculated as the median of the adjusted data from the individual instruments. Taking the median has the advantage of minimising the influence of outliers that might be present in the individual datasets.

Illustrations of original, adjusted and merged datasets in several latitude zones are presented in Figures 1 and 2, as well as in
205 Figures S1-S4 of the Supplement. These figures show that the adjustment procedure makes the datasets from individual datasets much closer to one another in period of overlapping measurements.

The uncertainty of the merged aerosol profiles are estimated similar to the approach used by Sofieva et al. (2017). For individual datasets, the uncertainty of the monthly mean values is estimated as the standard error of the mean, i.e., $\sigma_\beta^2 = \frac{s^2}{N}$, where s^2 is the sample variance and N is the number of measurements. The uncertainties of data adjustments are approximately
210 evaluated as uncertainty of bias computation and added quadratically to all individual monthly mean records except that of OSIRIS. The uncertainty of the merged aerosol extinction (which correspond to the median value β_{merged}) is estimated as (Sofieva et al., 2017):

$$\sigma_{\beta,merged} = min\left(\sigma_{\beta,i_{med}}, \sqrt{\frac{1}{N}\sum_{i=1}^{N}\sigma_{\beta,i}^2 + \frac{1}{N^2}\sum_{i=1}^{N}\left(\beta_{corr,i} - \beta_{merged}\right)^2}\right),$$
(5)

where $\sigma_{\beta,i_{med}}$ is the uncertainty of the extinction corresponding to the median value.
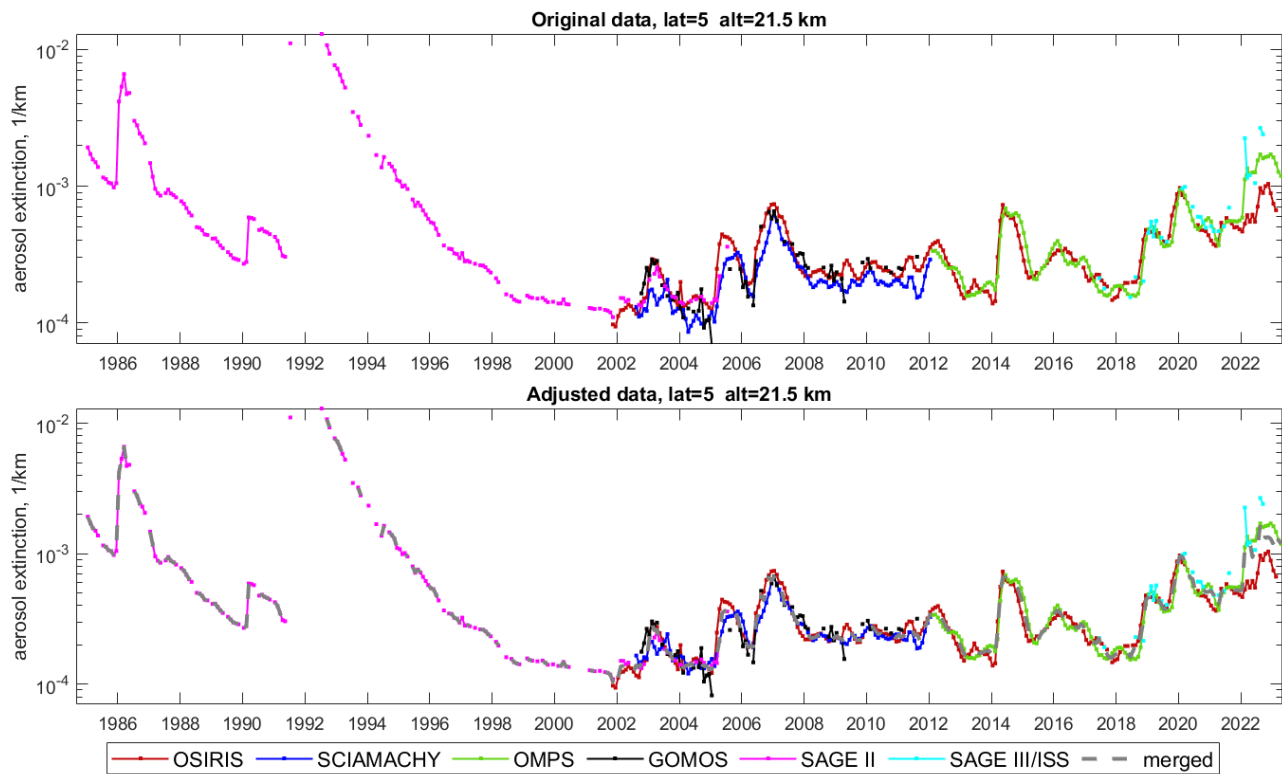
215

Figure 1. Aerosol extinction coefficient (1/km) at 21.5 km in the latitude zone 0–10°N. Colored lines correspond to aerosol records from individual instruments. Top panel: original data, bottom panel: adjusted data. The merged aerosol extinction coefficient is shown by grey line in the bottom panel.
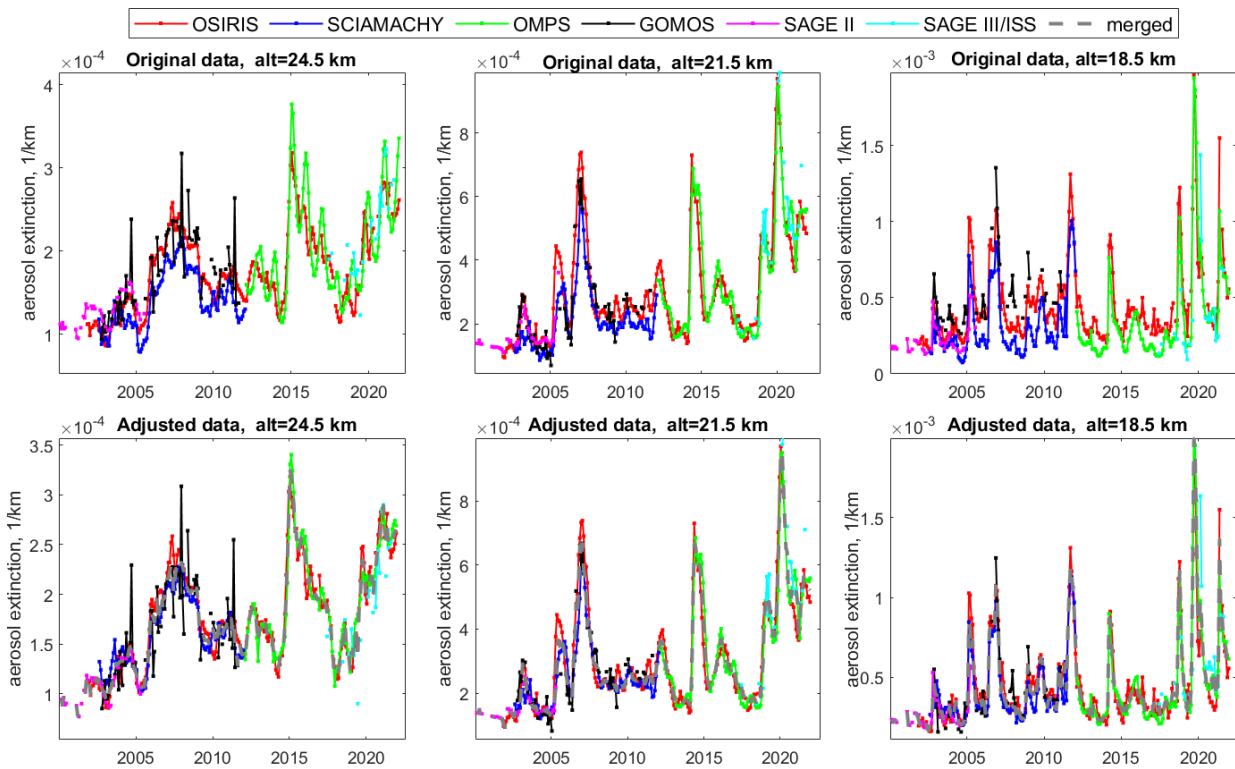
Figure 2. As Figure 1, but for several altitude levels and with the zoom on years 2000–2021.

Figure 3 shows the aerosol extinction profiles from the merged CREST dataset in three latitude zones, 30°–60°S (top), 20°S–20°N (center) and 30°–60°N (bottom). The main volcanic eruptions and strong wildfires are indicated in the figure with a bar of length proportional to the volcanic explosivity index (VEI). As observed in Figure 3, enhancements of aerosol extinction correspond to the enhanced volcanic activity or strong wildfires, which are listed in Table 2.
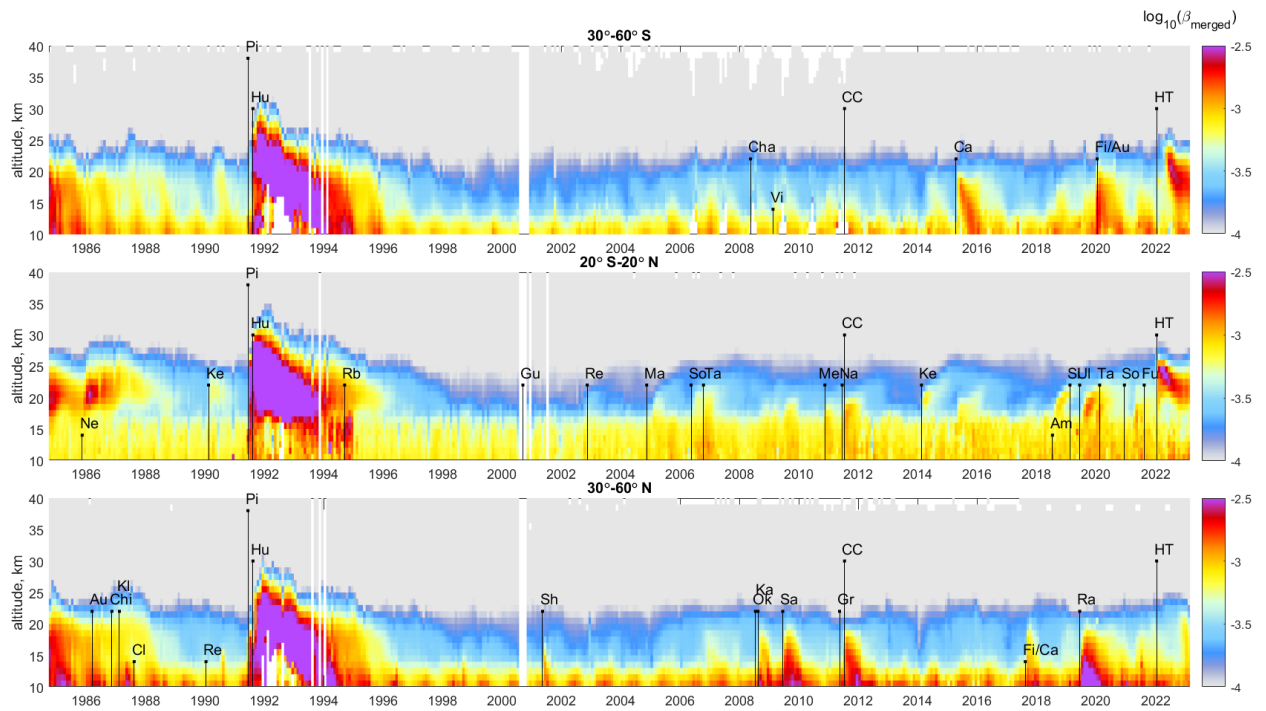
Figure 3. The CREST merged aerosol extinction profiles $\log_{10}(\beta_{merged}\,[\mathrm{km}^{-1}])$ **at 30°–60°S (top), 20°S–20°N (center) and 30°–60°N (bottom) . The volcanic eruptions are indicated by black bars with the length being proportional to the values of volcanic explosivity index (VEI). Volcanos with VEI>=5 are shown for all latitude zones, and with VEI>3 in the corresponding latitude zones.**

Table 2. The list of volcanic eruptions and strong wildfires, for which rise to the stratosphere.

Year	Month	Volcano/wildfire name	Abbreviation	Latitude (deg North)	VEI
1985	11	Nevado del Ruiz	Ne	5	3
1986	3	Augustine	Au	59	4
1986	11	Chikurachki	Chi	50	4
1987	2	Kliuchevskoi	Kl	56	4
1987	8	Cleveland	Cl	53	3
1990	1	Redoubt	Re	61	3
1990	2	Kelut	Ke	-8	4
1991	6	Pinatubo	Pi	15	6

1991	8	Mt.Hudson	Hu	-46	5
1994	9	Rabaul	Rb	-4	4
1999	8	Sheveluch	Sh	57	4
2000	9	Guagua Pichincha	Gu	0	4
2001	5	Shiveluch	Sh	56	4
2002	11	Reventador	Re	0	4
2004	11	Manam	Ma	4	4
2006	5	Soufrière Hills	So	16	4
2006	10	Rabaul/Tavurvur	Ta	-4	4
2008	5	Chaitén	Cha	-42	4
2008	7	Okmok	Ok	55	4
2008	8	Kasatochi	Ka	55	4
2009	2	Fire/Victoria	Vi	-37	3
2009	6	Sarychev	Sa	48	4
2010	11	Merapi	Me	-8	4
2011	5	Grimsvótn	Gr	64	4
2011	6	Nabro	Na	13	4
2011	7	Cordon Caulle	CC	-40	5
2014	2	Kelut	Ke	-8	4
2015	4	Calbuco	Ca	-41	4
2017	8	Wildfires/California	Fi/Ca	51	3
2018	7	Ambae	Am	-15	3
2019	2	Sinabung	Si	3	4
2019	6	Ulawun	Ul	-5	4
2019	6	Raikoke	Ra	48	4
2020	2	Taal	Ta	14	4
2020	1	Fire/Australia	Fi/Au	-35	4
2020	12	Soufriere St.Vincent	So	13	4
2021	8	Fukutoku-Oka-no-Ba	Fu	24	4
2022	1	HungaTonga-Hunga	HT	-21	5

4 Filling gaps in SAGE II data during Pinatubo

It has been reported in several publications that SAGE II aerosol load is underestimated or missing in the lower stratosphere during Pinatubo volcanic eruption (Kovilakam et al., 2020; Sukhodolov et al., 2018). The reason is "saturation" in SAGE II data, i.e., there are no values larger than ~0.012 km^{-1}. The GloSSAC dataset (Kovilakam et al., 2020; Thomason et al., 2018) uses experimentally scaled CLAES data at these times/locations. Instead, we applied the following approach in the merged CREST dataset. In the period affected by Pinatubo volcanic eruption, i.e., from June 1991 and lasting 3 years, the aerosol extinction $\beta(t)$ as a function of time for each altitude level is fitted by the function

$$f(t) = a + b\left(1 - \exp\left(-\frac{t}{\tau_1}\right)\right)\exp\left(-\frac{t}{\tau_2}\right), \tag{5}$$

where a, b, τ_1 and τ_2 are parameters to fit. Eq.(5) gives a simple parameterization of fast growing and gradual decrease; it is not linked with a dynamical model. The coefficient a is estimated as the mean over the period from January to May 1991, while other parameters are obtained via non-linear least-squares fitting by the Levenberg-Marquardt algorithm. As illustrated in Figure 4 (left) for 27.5 km, the aerosol peak associated with the Pinatubo eruption follows Eq. (5) well, for the cases where SAGE II data are not saturated. For lower altitudes (from the tropopause to the level 8 km above the tropopause), the data from 3 to 12 months after the Pinatubo eruption are not used in the fit, as illustrated in Figure 4 (right). The fitted aerosol peak during the strong Pinatubo load exceeds the maximal aerosol extinction value of ~0.012 km^{-1} reported by SAGE II. The period for omitting data, from 3 to 12 months after Pinatubo eruption, was selected after visual inspection, it corresponds to typical saturation period of nearly constant values. The fitting is performed in the stratosphere only, where there are a sufficient number of data points.

We performed such Pinatubo-filtering to the data in the tropics (20°S − 20°N) and in other latitude zones (20°− 40°, 40°− 60°, 60°− 90°, both North and South), and found that the saturation primarily affects the data in the tropics. Therefore, for latitude zones from 20°S to 20°N the saturated aerosol data (i.e., for altitudes below 26 km, where the fitted aerosol value exceeds 0.011 km^{-1}) are replaced with the fitted values. Missing data during Pinatubo eruption are also replaced with the fit.
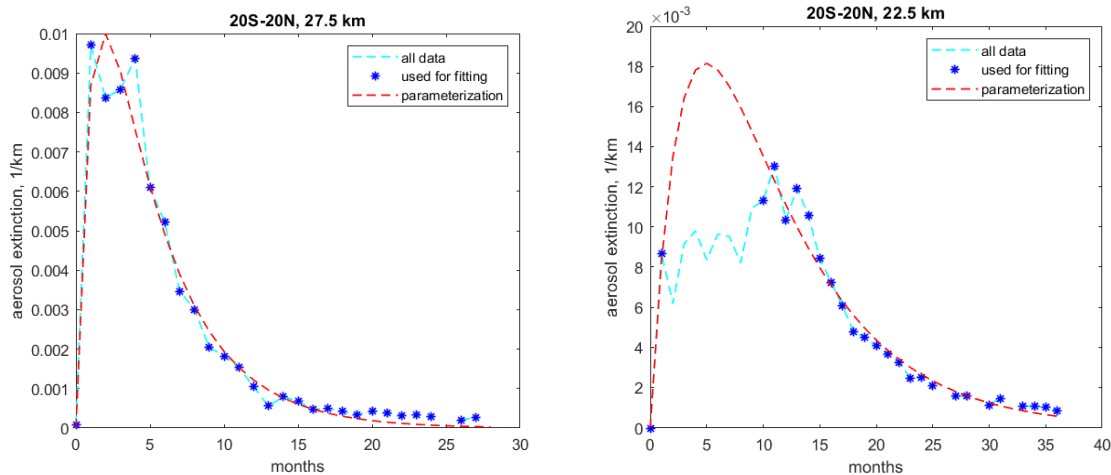
260 **Figure 4. Example of the SAGE II aerosol fitting during the Pinatubo period with the function Eq.(5) at 27.5 km (left) and 22.5 km (right). The data are for latitudes 20°S–20°N. For 27.5 km, all data used for the fit. For 22.5 km, the data from 3 to 10 months after Pinatubo eruption are excluded.**
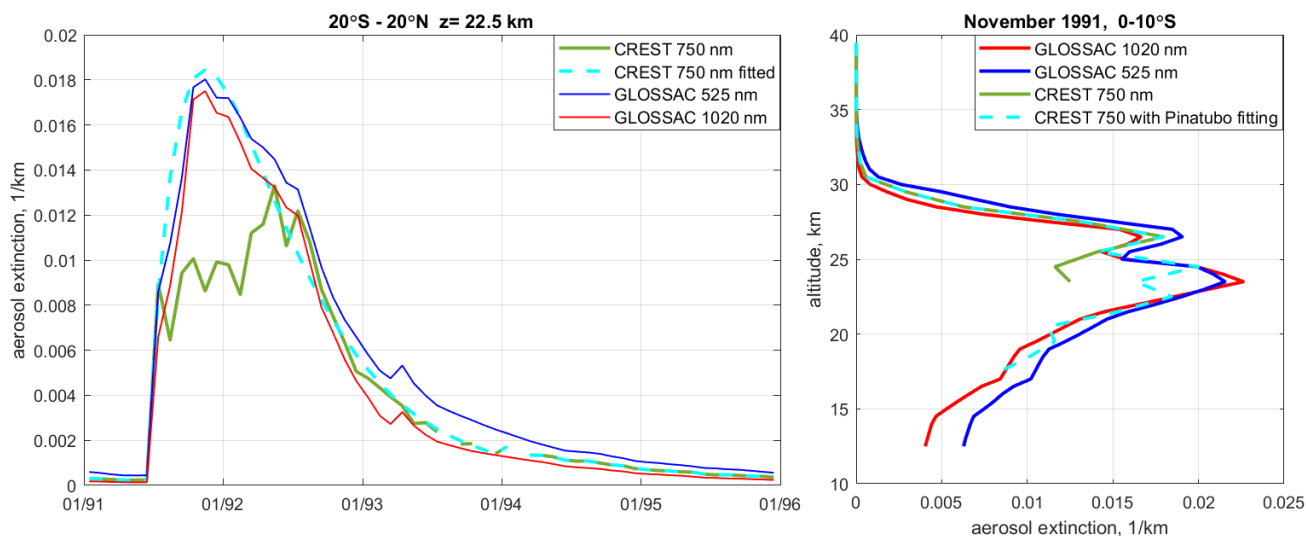
265 **Figure 5. Left: time series of aerosol extinction at 22.5 km as reported by GloSSAC (at 525 and 1020 nm) and CREST (original data (green solid line) and fitted by Eq.(5), cyan dashed line). Right: GloSSAC, CREST original and Pinatubo-corrected aerosol profiles in November 1991, in the latitude zone 0°–10°S.**

The resulting Pinatubo-corrected aerosol profiles agree with GloSSAC within 5-10%, as illustrated in Figure 5. Taking into account the uncertainty of gaps filling approaches during Pinatubo in GloSSAC and CREST, such an agreement can be
270 considered as very good. Unfortunately, there are no available in-situ measurements of aerosol extinction profiles during this period to validate CREST and GloSSAC profiles. However, the similarity between the GloSSAC and CREST aerosol profiles during the Pinatubo event increases confidence in both gap-filling approaches.

5 Creating stratospheric aerosol optical depth

275 The stratospheric aerosol optical depth (SAOD) has been computed via integration of aerosol extinction profiles from tropopause to ~40 km. The tropopause is computed using ERA-5 data according to the WMO definition of thermal tropopause. The resulting SAOD record is shown in Figure 6(a).
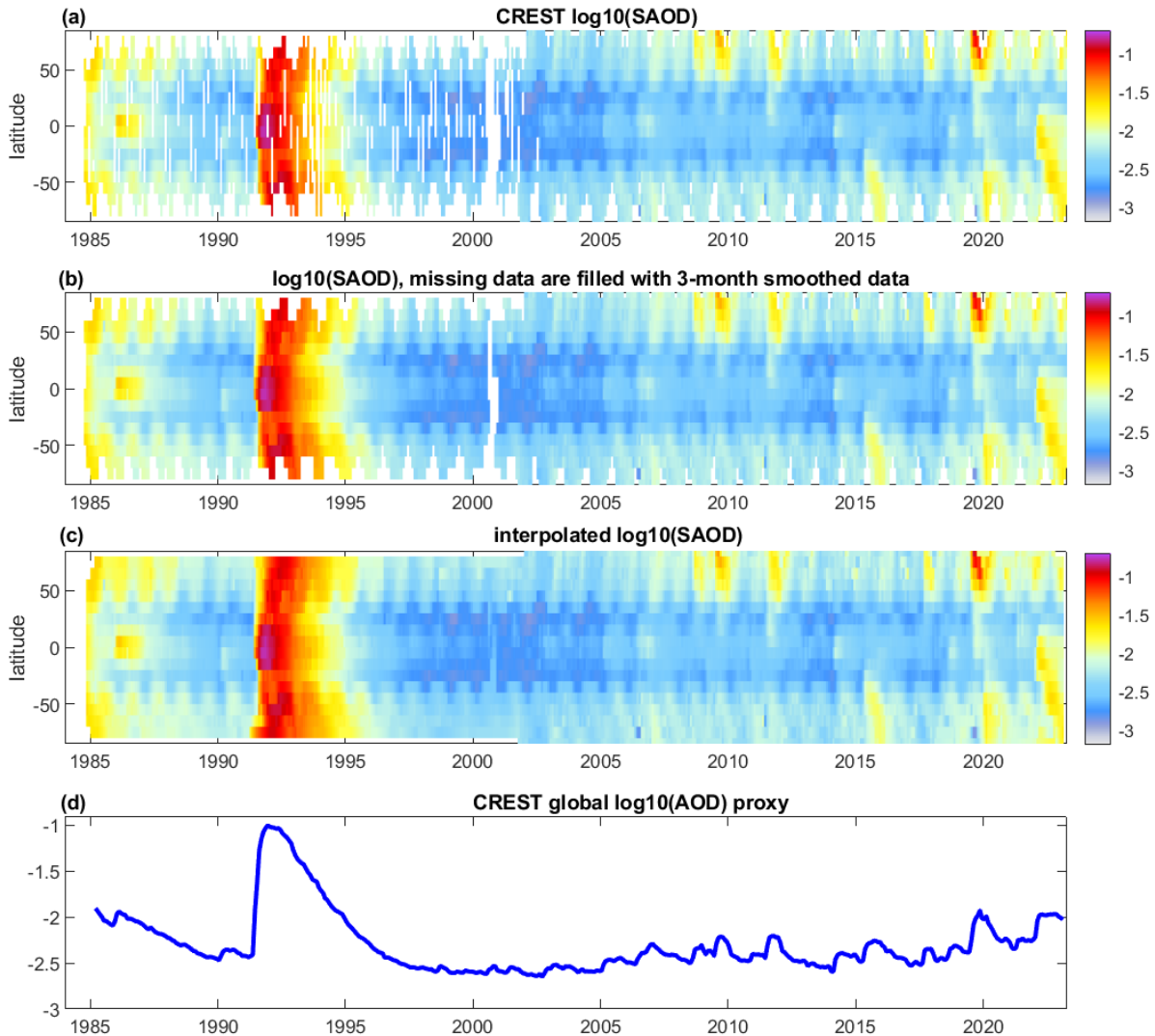
Figure 6.Illustration of creating CREST SAOD and aerosol proxy. (a) SAOD as obtained from the integration of aerosol profiles;
280 **(b) as (a) but missing data are filled in with the 3-month mean, for each latitude zone; (c) the gap-free SAOD obtained from (b) by interpolation by Delaney triangulation; (d) global mean SAOD (aerosol proxy). All SAOD values are plotted using logarithmic (log10) scales.**

285   The uncertainty of the stratospheric aerosol optical depth is evaluated using the error propagation.

For using SAOD in climate simulations and in trend analyses, a gap-free dataset is needed. For this, we first fill small gaps by smoothing the data in each latitude zone by applying a 3-month running average (Figure 6b). Then the Delaunay triangulation method is applied to the time-latitude SAOD field, resulting in gap-free stratospheric aerosol climate data record, which is illustrated in Figure 6c.

290   The global average (area-weighted) in the latitude range from 80°S – 80°N stratospheric aerosol optical depth is shown in Figure 6(d); it is used as aerosol proxy in e.g. trend analyses.

6   The merged CREST SAOD dataset: illustrations, comparison with GLOSSAC

The interpolated CREST SAOD dataset is shown in Figure 7(a), together with main aerosol events (volcanic eruptions and wildfires), which are indicated by black circles of the size proportional to their volcanic explosivity index VEI (Table 1). As

295   observed in Figure 7(a), aerosol enhancements match very well with volcanic eruptions and strong wildfires.

The comparison of CREST and GloSSAC stratospheric optical depth datasets is shown in Figure 7. GloSSAC provides SAOD at 525 nm and 1020 nm, therefore SAOD is higher for 525 nm and lower for 1020 nm than CREST SAOD. The overall morphology of SAOD enhancements is very similar (taking into account the wavelength-dependence) in CREST and

300   GloSSAC. The comparison of global mean SAOD from CREST (750 nm) and GloSSAC (525 nm and 1020 nm) is shown in Figure 8. The global mean was computed as area-weighted SAOD in latitude range from 80° S to 80°N. In this figure, we show also global GloSSAC SAOD converted to 750 nm by using the same method as applied to SAGE II data (see Sect. 3). As seen in Figure 8, CREST and GloSSAC aerosol proxies are in very good agreement and show expected wavelength dependence of aerosol extinction. At the peak of Pinatubo the CREST global SAOD is slightly different from that converted

305   from the GloSSAC SAOD, which is probably related to different fitting/scaling of SAGE II data used in CREST and GloSSAC.
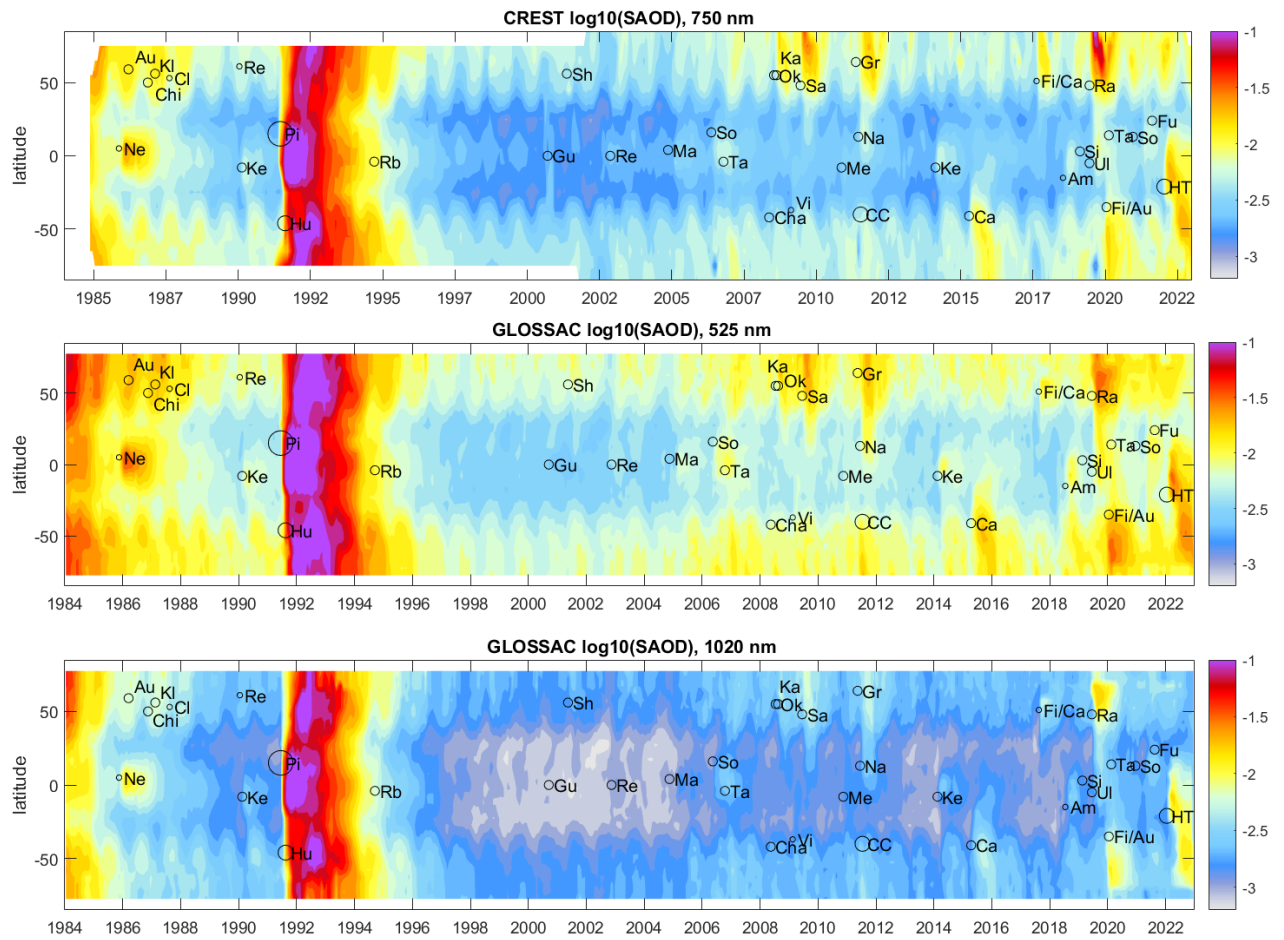
Figure 7. CREST SAOD at 750 nm (top), GloSSAC SAOD at 525nm (center), and GloSSAC SAOD at 1020 nm (bottom). SAOD is presented in logarithmic color scale. Volcanic eruptions and wildfires are indicated by black circles of the size proportional to their volcanic explosivity index VEI (Table 1).
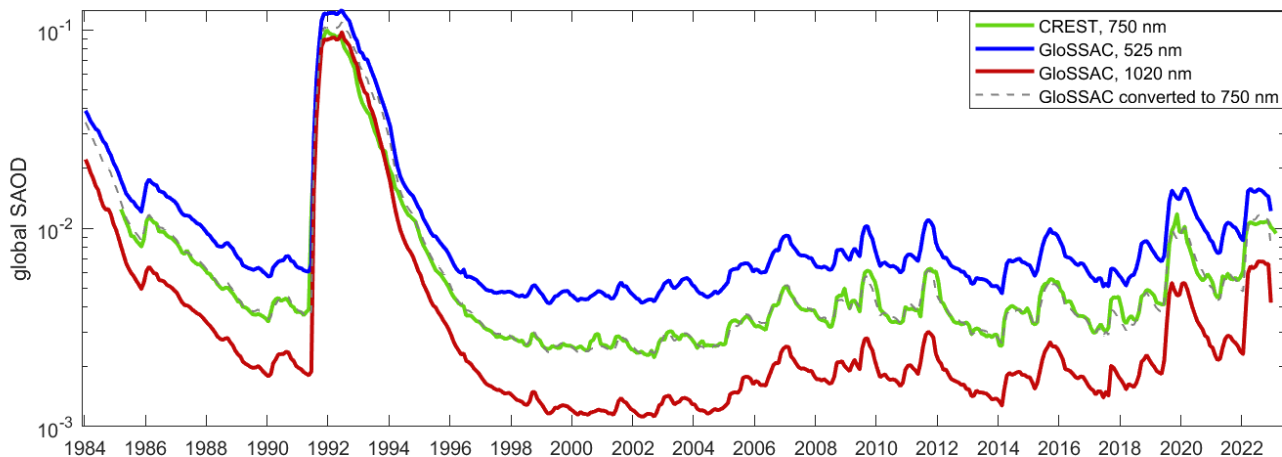
Figure 8. Global mean stratospheric optical depth from CREST (750 nm) and GloSSAC (525 and 1020 nm).

7   Summary and discussion

315   In this paper, we presented a new climate data record of stratospheric aerosols (CREST). The merged CREST dataset includes:

- Monthly zonal mean aerosol extinction profiles at 750 nm from 8.5 to 39.5 km in 10° latitudinal bins from 90°S to 90°N
- Monthly zonal mean stratospheric aerosol optical depth at 750 nm in 10° latitudinal bins from 90°S to 90°N
- Global mean stratospheric optical depth, which can be used as an aerosol proxy in trend analyses.

320   The CREST data set combines the data from six limb and occultation instruments: OSIRIS, SAGE II, SAGE III/ISS, SCIAMACHY, OMPS-LP, and GOMOS. The CREST dataset is complementary to NASA-GloSSAC: it provides aerosols at a different wavelength, 750 nm, it uses a different collection of individual datasets included in the merged dataset and a different merging approach. In addition, a different correction of saturated SAGE II data during Pinatubo period is applied in construction of the CREST dataset. The overall agreement between the CREST and GloSSAC SAOD is very good.

325   The CREST dataset is in open access at https://fmi.b2share.csc.fi/records/8bfa485de30840eba42d1d407f4ce19c. At the moment, it covers the period from October 1984 to December 2023, and it is intended to be extended in the future.

The created merged dataset of aerosol profiles can be used in various climate-related studies. For example, it can be used as a proxy in the regression models for trend analyses, or as a forcing in simulations with chemistry-transport models.

For the CREST dataset, we used aerosol extinction profiles from instruments measuring in the limb-viewing
330   geometry, and compared it with GloSSAC, which uses similar measurements. When new limb aerosol extinction profiles will be available, they can be easily added to the merged dataset using the methods explained in the paper. However, there are also several   active   remote   sensing   instruments,   such   as   CALIPSO,   Aeolus

(https://www.esa.int/Applications/Observing_the_Earth/FutureEO/Aeolus, Flament et al., 2021), and EarthCARE
(https://www.esa.int/Applications/Observing_the_Earth/FutureEO/EarthCARE), which provide aerosol profiles from
335   measurements in the nadir-viewing geometry. The quantities measured by active instruments (backscattering ratio) and
sampling (about a hundred meters wide footprint stripe vs. several hundred kilometers large footprints of limb instruments)
are very different to those from the instruments used in this study. These differences in the measurement principles result in
different sensitivity to aerosols and vertical range of retrieved aerosol profiles. Nevertheless, comparison of aerosol climate
data records from limb and nadir measurement systems would provide added value increasing the reliability of the stratospheric
340   aerosol climate data record. Such an interesting and challenging task can be implemented in future works.

Data availability

The merged CREST aerosol dataset (Sofieva, et al., 2022) is available at
https://fmi.b2share.csc.fi/records/8bfa485de30840eba42d1d407f4ce19c. The original version (v1,
345   https://doi.org/10.23728/fmi-b2share.8bfa485de30840eba42d1d407f4ce19c) is until May 2022, while the extended version
(v2, https://doi.org/10.57707/fmi-b2share.dfe14351fd8548bcaca3c2956b17f665) is until December 2023. Interested readers
can ask for the computational code from the corresponding author.

Author contributions
350   VFS and AR designed the study and performed the analyses, VFS wrote the majority of the paper. MS
collected the database of volcanic eruptions. AR, JPB, CR, RD, DD, LAR and AB provided the data and contributed
to the analyses and writing of the paper.

Competing interests

The contact author has declared that none of the authors has any competing interests.

355   **Acknowledgements**

The work is performed in the framework of ESA project CREST. The creation of the SCIAMACHY and OMPS-LP aerosol
data sets at the University of Bremen was funded in parts by ESA via CREST project, by the German Research Foundation
(DFG) via the Research Unit VolImpact (grant no. FOR2820), and by the University and State of Bremen. The University of
Bremen team gratefully acknowledges the computing time granted by the Resource Allocation Board and provided on the
360   supercomputer Lise and Emmy at NHR@ZIB and NHR@Göttingen as part of the NHR infrastructure. The calculations for

this research were conducted with computing resources under the project hbk00098. The FMI team thanks the Academy of Finland (Centre of Excellence of Inverse Modelling and Imaging; decision 353082).

References

Bertaux, J.-L., Kyrölä, E., Fussen, D., Hauchecorne, A., Dalaudier, F., Sofieva, V. F., Tamminen, J., Vanhellemont, F.,
365 D'Andon, O. F., Barrot, G., Mangin, A., Blanot, L., Lebrun, J. C., Pérot, K., Fehr, T., Saavedra, L., Leppelmeier, G. W., and Fraisse, R.: Global ozone monitoring by occultation of stars: an overview of GOMOS measurements on ENVISAT, Atmos. Chem. Phys., 10, 12091–12148, https://doi.org/10.5194/acp-10-12091-2010, 2010.

Bourassa, A. E., Rieger, L. A., Lloyd, N. D., and Degenstein, D. A.: Odin-OSIRIS stratospheric aerosol data product and SAGE III intercomparison, Atmospheric Chemistry and Physics, 12, 605–614, https://doi.org/10.5194/acp-12-605-2012, 2012.

370 Bovensmann, H., Burrows, J. P., Buchwitz, M., Frerick, J., Noël, S., Rozanov, V. V., Chance, K. V., and Goede, A. P. H.: SCIAMACHY: Mission Objectives and Measurement Modes, Journal of the Atmospheric Sciences, 56, 127–150, https://doi.org/10.1175/1520-0469(1999)056<0127:SMOAMM>2.0.CO;2, 1999.

Burrows, J. P., Hölzle, E., Goede, A. P. H., Visser, H., and Fricke, W.: SCIAMACHY—scanning imaging absorption spectrometer for atmospheric chartography, Acta Astronautica, 35, 445–451, http://dx.doi.org/10.1016/0094-5765(94)00278-
375 T, 1995.

Crutzen, P. J.: Albedo Enhancement by Stratospheric Sulfur Injections: A Contribution to Resolve a Policy Dilemma?, Climatic Change, 77, 211, https://doi.org/10.1007/s10584-006-9101-y, 2006.

Damadeo, R. P., Zawodny, J. M., Thomason, L. W., and Iyer, N.: SAGE version 7.0 algorithm: application to SAGE II, Atmospheric Measurement Techniques, 6, 3539–3561, https://doi.org/10.5194/amt-6-3539-2013, 2013.

380 Damadeo, R. P., Sofieva, V. F., Rozanov, A., and Thomason, L. W.: An Empirical Characterization of the Aerosol Ångström Exponent Interpolation Bias using SAGE III/ISS Data, Atmospheric Measurement Techniques Discussions, 2023, 1–13, https://doi.org/10.5194/amt-2023-260, 2023.

Damadeo, R. P., Sofieva, V. F., Rozanov, A., and Thomason, L. W.: An empirical characterization of the aerosol Ångström exponent interpolation bias using SAGE III/ISS data, Atmos. Meas. Tech., 17, 3669–3678, https://doi.org/10.5194/amt-17-
385 3669-2024, 2024.

Davis, S. M., Damadeo, R., Flittner, D., Rosenlof, K. H., Park, M., Randel, W. J., Hall, E. G., Huber, D., Hurst, D. F., Jordan, A. F., Kizer, S., Millan, L. F., Selkirk, H., Taha, G., Walker, K. A., and Vömel, H.: Validation of SAGE III/ISS Solar Water Vapor Data With Correlative Satellite and Balloon-Borne Measurements, JGR Atmospheres, 126, e2020JD033803, https://doi.org/10.1029/2020JD033803, 2021.

390 Deshler, T.: A review of global stratospheric aerosol: Measurements, importance, life cycle, and local stratospheric aerosol, Atmospheric Research, 90, 223–232, http://dx.doi.org/10.1016/j.atmosres.2008.03.016, 2008.

Flament, T., Trapon, D., Lacour, A., Dabas, A., Ehlers, F., and Huber, D.: Aeolus L2A aerosol optical properties product: standard correct algorithm and Mie correct algorithm, Atmos. Meas. Tech., 14, 7851–7871, https://doi.org/10.5194/amt-14-7851-2021, 2021.

395   Flynn, L., Long, C., Wu, X., Evans, R., Beck, C. T., Petropavlovskikh, I., McConville, G., Yu, W., Zhang, Z., Niu, J., Beach, E., Hao, Y., Pan, C., Sen, B., Novicki, M., Zhou, S., and Seftor, C.: Performance of the Ozone Mapping and Profiler Suite (OMPS) products: OMPS OZONE PRODUCTS, J. Geophys. Res. Atmos., 119, 6181–6195, https://doi.org/10.1002/2013JD020467, 2014.

Kovilakam, M., Thomason, L. W., Ernest, N., Rieger, L., Bourassa, A., and Millán, L.: The Global Space-based Stratospheric
400   Aerosol Climatology (version 2.0): 1979–2018, Earth Syst. Sci. Data, 12, 2607–2634, https://doi.org/10.5194/essd-12-2607-2020, 2020.

Kyrölä, E., Tamminen, J., Leppelmeier, G. W., Sofieva, V. F., Hassinen, S., Bertaux, J.-L., Hauchecorne, A., Dalaudier, F., Cot, C., Korablev, O., D'Andon, O. F., Barrot, G., Mangin, A., Theodore, B., Guirlet, M., Etanchaud, F., Snoij, P., Koopman, R., Saavedra, L., Fraisse, R., Fussen, D., and Vanhellemont, F.: GOMOS on Envisat: An overview, Adv. Space Res., 33, 1020–
405   1028, 2004.

Kyrölä, E., Tamminen, J., Sofieva, V. F., Bertaux, J.-L., Hauchecorne, A., Dalaudier, F., Fussen, D., Vanhellemont, F., D'Andon, O. F., Barrot, G., Guirlet, M., Mangin, A., Blanot, L., Fehr, T., Miguel, L. de, and Fraisse, R.: Retrieval of atmospheric parameters from GOMOS data, Atmos. Chem. Phys., 10, 11881–11903, https://doi.org/10.5194/acp-10-11881-2010, 2010.

410   Llewellyn, E., Lloyd, N. D., Degenstein, D. A., Gattinger, R. L., Petelina, S. V., Bourassa, A. E., Wiensz, J. T., Ivanov, E. V., McDade, I. C., Solheim, B. H., McConnell, J. C., Haley, C. S., Savigny, C. von, Sioris, C. E., McLinden, C. A., Griffioen, E., Kaminski, J., Evans, W. F. J., Puckrin, E., Strong, K., Wehrle, V., Hum, R. H., Kendall, D. J. W., Matsushita, J., Murtagh, D. P., Brohede, S., Stegman, J., Witt, G., Barnes, G., Payne, W. F., Piche, L., Smith, K., Warshaw, G., Deslauniers, D. L., Marchand, P., Richardson, E. H., King, R. A., Wevers, I., McCreath, W., Kyrola, E., Oikarinen, L., Leppelmeier, G. W.,
415   Auvinen, H., Megie, G., Hauchecorne, A., Lefevre, F., Noe, J. de L., Ricaud, P., Frisk, U., Sjoberg, F., Scheele, F. von, and Nordh, L.: The OSIRIS instrument on the Odin spacecraft, Canadian Journal of Physics, 82, 411–422, https://doi.org/10.1139/p04-005, 2004.

Loughman, R., Bhartia, P. K., Chen, Z., Xu, P., Nyaku, E., and Taha, G.: The Ozone Mapping and Profiler Suite (OMPS) Limb Profiler (LP) Version 1 aerosol extinction retrieval algorithm: theoretical basis, Atmos. Meas. Tech., 11, 2633–2651,
420   https://doi.org/10.5194/amt-11-2633-2018, 2018.

Malinina, E., Rozanov, A., Rieger, L., Bourassa, A., Bovensmann, H., Burrows, J. P., and Degenstein, D.: Stratospheric aerosol characteristics from space-borne observations: extinction coefficient and Ångström exponent, Atmos. Meas. Tech., 12, 3485–3502, https://doi.org/10.5194/amt-12-3485-2019, 2019.

Pohl, C., Wrana, F., Rozanov, A., Deshler, T., Malinina, E., Von Savigny, C., Rieger, L. A., Bourassa, A. E., and Burrows, J.
425   P.: Stratospheric aerosol characteristics from SCIAMACHY limb observations: two-parameter retrieval, Atmos. Meas. Tech., 17, 4153–4181, https://doi.org/10.5194/amt-17-4153-2024, 2024.

Rieger, L. A., Bourassa, A. E., and Degenstein, D. A.: Merging the OSIRIS and SAGE II stratospheric aerosol records, J. Geophys. Res. Atmos., 120, 8890–8904, https://doi.org/10.1002/2015JD023133, 2015.

Rieger, L. A., Malinina, E. P., Rozanov, A. V., Burrows, J. P., Bourassa, A. E., and Degenstein, D. A.: A study of the
430   approaches used to retrieve aerosol extinction, as applied to limb observations made by OSIRIS and SCIAMACHY, Atmos. Meas. Tech., 11, 3433–3445, https://doi.org/10.5194/amt-11-3433-2018, 2018.

Rieger, L. A., Zawada, D. J., Bourassa, A. E., and Degenstein, D. A.: A Multiwavelength Retrieval Approach for Improved OSIRIS Aerosol Extinction Retrievals, J. Geophys. Res. Atmos., 2018JD029897, https://doi.org/10.1029/2018JD029897, 2019.

435   Rozanov, A., Pohl, C., Arosio, C., Bourassa, A., Bramstedt, K., Malinina, E., Rieger, L., and Burrows, J. P.: Retrieval of stratospheric aerosol extinction coefficients from OMPS-LP measurements, https://doi.org/10.5194/egusphere-2024-358, 8 February 2024.

Russell, P. B. and McCormick, M. P.: SAGE II aerosol data validation and initial data use: An introduction and overview, J. Geophys. Res., 94, 8335–8338, https://doi.org/10.1029/JD094iD06p08335, 1989.

440   von Savigny, C., Ernst, F., Rozanov, A., Hommel, R., Eichmann, K.-U., Rozanov, V., Burrows, J. P., and Thomason, L. W.: Improved stratospheric aerosol extinction profiles from SCIAMACHY: validation and sample results, Atmos. Meas. Tech., 8, 5223–5235, https://doi.org/10.5194/amt-8-5223-2015, 2015.

Sofieva, V. F., Kyrölä, E., Laine, M., Tamminen, J., Degenstein, D., Bourassa, A., Roth, C., Zawada, D., Weber, M., Rozanov, A., Rahpoe, N., Stiller, G., Laeng, A., Clarmann, T. von, Walker, K. A., Sheese, P., Hubert, D., Roozendael, M. van, Zehner, 445   C., Damadeo, R., Zawodny, J., Kramarova, N., and Bhartia, P. K.: Merged SAGE II, Ozone_cci and OMPS ozone profile dataset and evaluation of ozone trends in the stratosphere, Atmospheric Chemistry and Physics, 17, 12533–12552, https://doi.org/10.5194/acp-17-12533-2017, 2017.

Sofieva, V. F., Szelag, M., Tamminen, J., Fussen, D., Bingen, C., Vanhellemont, F., Mateshvili, N., Rozanov, A., and Pohl, C.: Multi-wavelength dataset of aerosol extinction profiles retrieved from GOMOS stellar occultation measurements, Atmos. 450   Meas. Tech., 17, 3085–3101, https://doi.org/10.5194/amt-17-3085-2024, 2024.

Sofieva, V.F., Rozanov, A., and Szelag, M.: Merged aerosol extinction profiles and stratospheric optical depth dataset created using data from several satellite limb and occultation instrumentsClimate data Record of Stratospheric aerosols (CREST) (1.0), https://doi.org/10.23728/FMI-B2SHARE.8BFA485DE30840EBA42D1D407F4CE19C, 2022.

Sukhodolov, T., Sheng, J.-X., Feinberg, A., Luo, B.-P., Peter, T., Revell, L., Stenke, A., Weisenstein, D. K., and Rozanov, E.: 455   Stratospheric aerosol evolution after Pinatubo simulated with a coupled size-resolved aerosol–chemistry–climate model, SOCOL-AERv1.0, Geosci. Model Dev., 11, 2633–2647, https://doi.org/10.5194/gmd-11-2633-2018, 2018.

Thomason, L. W., Burton, S. P., Luo, B.-P., and Peter, T.: SAGE II measurements of stratospheric aerosol properties at non-volcanic levels, Atmospheric Chemistry and Physics, 8, 983–995, https://doi.org/10.5194/acp-8-983-2008, 2008.

Thomason, L. W., Ernest, N., Millán, L., Rieger, L., Bourassa, A., Vernier, J.-P., Manney, G., Luo, B., Arfeuille, F., and Peter, 460   T.: A global space-based stratospheric aerosol climatology: 1979–2016, Earth System Science Data, 10, 469–492, https://doi.org/10.5194/essd-10-469-2018, 2018a.

Thomason, L. W., Ernest, N., Millán, L., Rieger, L., Bourassa, A., Vernier, J.-P., Manney, G., Luo, B., Arfeuille, F., and Peter, T.: A global space-based stratospheric aerosol climatology: 1979--2016, Earth System Science Data, 10, 469–492, https://doi.org/10.5194/essd-10-469-2018, 2018b.

465   Vanhellemont, F., Fussen, D., Mateshvili, N., Tetard, C., Bingen, C., Dekemper, E., Loodts, N., Kyrola, E., Sofieva, V. F., Tamminen, J., Hauchecorne, A., Bertaux, J.-L., Dalaudier, F., Blanot, L., D'Andon, O. F., Barrot, G., Guirlet, M., Fehr, T., and Saavedra, L.: Optical extinction by upper tropospheric/stratospheric aerosols and clouds: GOMOS observations for the period 2002-2008, ATMOSPHERIC CHEMISTRY AND PHYSICS, 10, 7997–8009, https://doi.org/10.5194/acp-10-7997-2010, 2010.

470   Vernier, J.-P., Thomason, L. W., Pommereau, J.-P., Bourassa, A., Pelon, J., Garnier, A., Hauchecorne, A., Blanot, L., Trepte, C., Degenstein, D., and Vargas, F.: Major influence of tropical volcanic eruptions on the stratospheric aerosol layer during the last decade, Geophysical Research Letters, 38, https://doi.org/10.1029/2011GL047563, 2011.

Wang, H. J., Cunnold, D. M., Thomason, L. W., Zawodny, J. M., and Bodeker, G. E.: Assessment of SAGE version 6.1 ozone data quality, Journal of Geophysical Research: Atmospheres, 107, ACH 8-1-ACH 8-18, https://doi.org/10.1029/2002JD002418, 2002.

Wang, H. J. R., Damadeo, R., Flittner, D., Kramarova, N., Taha, G., Davis, S., Thompson, A. M., Strahan, S., Wang, Y., Froidevaux, L., Degenstein, D., Bourassa, A., Steinbrecht, W., Walker, K. A., Querel, R., Leblanc, T., Godin-Beekmann, S., Hurst, D., and Hall, E.: Validation of SAGE III/ISS Solar Occultation Ozone Products With Correlative Satellite and Ground-Based Measurements, Journal of Geophysical Research: Atmospheres, 125, e2020JD032430, https://doi.org/10.1029/2020JD032430, 2020.